



Full Length Article

Widening the operation limits of a SI engine running on neat ammonia

Mads Carsten Jespersen, Thomas Østerby Holst Rasmussen, Anders Ivarsson *

Technical University of Denmark, Department of Civil and Mechanical Engineering, Kgs. Lyngby, Denmark

A B S T R A C T

Present study aims to investigate the lean-burn characteristics of ammonia in a pre-mixed SI (Spark Ignition) engine and the influence of spark energy and discharge characteristics on engine performance and emissions. A wide range of engine operation conditions have been explored with particular focus on emission measurement. Engine parameters have been systematically swept to explore engine control strategies that would be operational in real engine application with a wide range of engine loads and tight emission regulations.

Most previous studies required more than 5 % addition of hydrogen to the ammonia in order to achieve stable ignition for wide operation conditions. This has been a major obstacle in the application of ammonia for SI engines due to safety and system complexity issues. In present work, a comprehensive effort was made to understand and optimize the spark ignition system in order to mitigate the need for an ignition improver and all experiments have been performed with 100 % neat ammonia.

With present engine modifications, emissions of unburned ammonia was measured to be between 5000 and 10000 ppm and with a combustion efficiency above 95 %. The unburned ammonia is believed to originate from crevices, particularly at the ring-pack. The NO_x emission was between 4000 and 8000 ppm even at high excess air ratios. The emission of N₂O is critical to minimize, as it is a strong greenhouse gas. It was measured to be between 20 and 80 ppm and appear to be related to post oxidation reactions of ammonia released from crevices during expansion.

Advancing the ignition timing has proved to be an efficient handle for balancing the emissions of NH₃ and NO_x. These emissions will be reduced to H₂O and N₂ in an SCR catalyst if they are correctly balanced. Fortunately, advancing ignition timing also minimizes the formation of N₂O.

1. Introduction

Ammonia is gaining attention as an ICE (Internal Combustion Engine) fuel because it is one of the most cost-efficient ways to carry and store renewable hydrogen and it is carbon free [1]. The internal combustion engine community is interested in ammonia as it can be utilized directly in the engine without conversion to hydrogen, and the infrastructure already exists as it is one of the most produced and transported chemicals [1]. Thus, ammonia can facilitate the introduction of hydrogen into the existing vast infrastructure propelled by cost effective internal combustion engines, extending to ship propulsion, road transport and peak power production.

Due to the reluctance of ammonia to auto ignite and the high latent heat, a premixed-type combustion process is favorable. The reluctance to auto-ignite not only motivates a premixed combustion, but also enables a high compression ratio without undesired occurrences of pre-ignition or excessive knocking. In addition, high intake pressure proves to be beneficial for combustion quality. Ammonia's ability to withstand high compression ratios and high intake pressures increases the potential power density of a commercial ammonia fueled engine.

1.1. Ammonia engine history

The use of ammonia as a fuel for the ICE (Internal Combustion Engine) has been studied since the 1960's [2]. SI (Spark Ignition) and CI (Compression Ignition) combustion concepts have been tested experimentally by multiple authors. For neat ammonia SI engine operation, studies have investigated the influence of ignition energy, and found that the choice of ignition system is critical to engine performance [3,4,5]. Most studies reported about poor engine performance for 100 % ammonia operation and deem neat ammonia suboptimal as an engine fuel without the addition of an ignition promoter i.e., hydrogen. Experimental campaigns carried out using the same CFR engine as the present study have contributed to those conclusions, reporting that satisfactory engine performance using neat ammonia was unfeasible [6,7,8]. These and most other previous studies concluded that more than 5 % addition of hydrogen to the ammonia was required to achieve stable ignition for wide operation conditions. This has been a major obstacle in the practical application of ammonia for SI engines due to safety and system complexity issues.

However, few recent studies have found 100 % ammonia operation to be possible with low cyclic variation [9,10] at rather narrow

* Corresponding author.

E-mail address: aniv@dtu.dk (A. Ivarsson).

operating conditions. These studies had another focus than neat ammonia combustion and thus have not investigated combustion characteristics for leaner mixtures ($\lambda > 1.1$) and the influence of ignition energy and spark characteristics was not explored.

1.2. Ammonia ignition

The required ignition energy for neat ammonia in laboratory tests has been reported to be in the range of 8–680 mJ, which is a wide range on a significantly higher level than that of hydrocarbons [4]. This challenge has, since the beginning of ammonia application in ICEs, raised the question whether neat ammonia would work as an engine fuel. Pearsall [4] investigated the influence of ignition energy on ammonia ignition in engines and concluded that higher than conventional spark energy and longer spark duration are favorable. He reported that an ignition energy of 52 mJ with a spark duration of 0.5 ms is superior to shorter capacitive discharges of duration 0.02–0.07 ms with similar discharge energy. Cornelius et al. [3] tested premixed spark ignition of ammonia for multiple engine layouts and found MBT (Maximum Break Torque) spark timing to be around –100 CAD. Even with modifications to the applied ignition system for higher spark energy, successful combustion of ammonia required highly advanced ignition timing. Improvements were however observed with increased cylinder temperature, pressure, and turbulence, where piston shape also induced combustion improvements. Poor indicated thermal efficiencies at part load operation led to the conclusion that hydrogen addition would be necessary for part load operation.

Present study only concerns spark ignition but previous studies have tested various types of dual fuel concepts used to ignite premixed ammonia in engines [2]. More recently, experiments showed that neat, pre-mixed ammonia could be properly ignited with a direct injection of only 1.5 % n-Heptane on energy basis [11]. Most other studies obtaining successful ignition of pre-mixed ammonia with direct injection of diesel but required a larger fraction of pilot fuel particular at lean condition [12,13]. Successful ignition of neat, pre-mixed ammonia has also been achieved with a pre-chamber using hydrogen, methane or gasoline in the pre-chamber [14]. Hydrogen gave best results and could provide stable operation at lean conditions up to $\lambda = 1.4$.

1.3. Emissions from ammonia combustion

A well-known challenge with premixed engines is the release of unburned fuel that was trapped in crevices during combustion [15]. This has always been a challenge for all premixed engines and all types of fuel. For typical hydrocarbon fuels, this problem is seen as loss of efficiency because the fuel trapped in the crevices is not burned in the main combustion but partly oxidizes later in the expansion stroke when it escapes the crevices [16]. An efficient way to reduce emissions of unburned and partly oxidized fuel is to reduce the piston top-land crevices as reported by [15,16,17]. Alkidas have reported that 1 % change of top-land crevice volume would lead to a 0.2 %-0.6 % decrease in HC [15]. The oxidation temperature of ammonia is much higher than that of typical hydrocarbon fuels and a larger part of the ammonia trapped in crevice volumes will therefore not be post-oxidize. Ammonia released from engine crevices will therefore constitute the main contribution to ammonia slip from an engine with an otherwise complete combustion of the bulk gas.

An efficient way to remove ammonia in after treatment is by reaction with NO_x in a SCR (Selective Catalytic Reduction) catalyst. One molecule of ammonia with one molecule of nitric oxide, NO, and oxygen is converted into water and nitrogen. It is therefore desired to have an engine out emission with NH₃/NO_x = 1 in order to efficiently reduce both NH₃ and NO_x.

Another concern with ammonia combustion is the emission of nitrous oxide, N₂O. Nitrous oxide is a strong greenhouse gas with a global warming potential of 310 in mass equivalents of CO₂ on a 100



Fig. 1. CFR engine setup used in present work.

year basis.

At moderate temperatures and in excess of oxygen the forward reaction of (1) is dominating the formation of N₂O in post-oxidation of ammonia released from crevices [7].



Earlier studies on NH₂/NO₂ reaction kinetics have lately been reconfirmed with new experimental data and conclude that N₂O formation starts to increase via (1) with decreasing temperature around 1350 K [18,19]. At higher temperatures with excess of oxygen, the consumption of NH₂ radical is dominated by (2) without formation of N₂O. At lower temperatures around 650 K all reactions start to quench due low radical formations.

These intermediate temperatures will inevitably be present during expansion when trapped ammonia is released from the crevice and result in formation of N₂O.

1.4. This work

The present study aims to investigate the lean-burn characteristics of ammonia in an SI engine and the influence of spark energy and discharge characteristics on engine performance and emissions. A wide range of engine operation conditions have been explored with particular focus on emission measurement. Engine parameters have been systematically swept to explore engine control strategies that would be operational in real engine application with a wide range of engine loads and

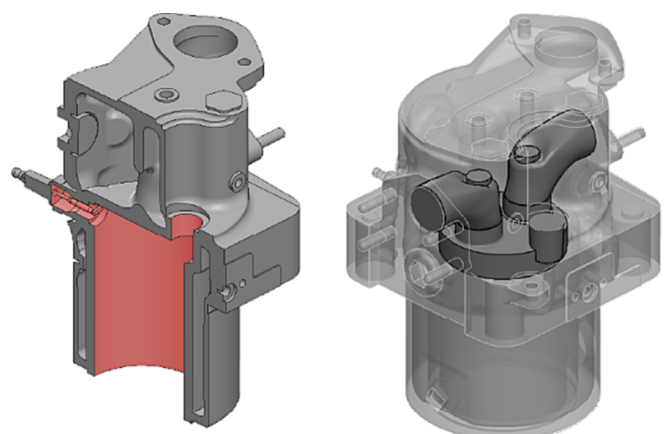


Fig. 2. CAD model of cylinder head and liner based on a 3D scan of similar CFR engine [21].

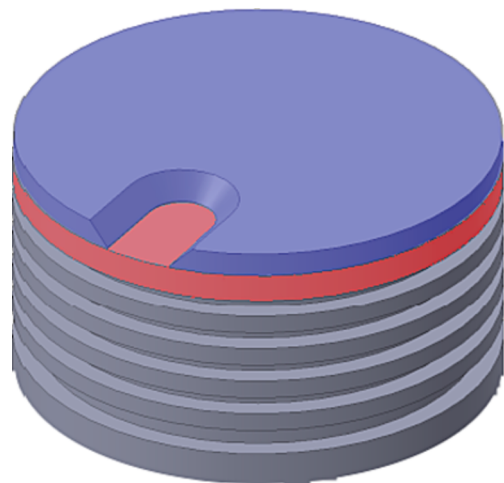


Fig. 3. CAD model of CFR piston with added piston top [22].

Table 1
CFR engine specifications.

Bore	82.78 mm
Stroke	114.3 mm
Compression ratio	4.5–15
Intake pressure	0.5–1.5 bar absolute
Valves	Shrouded intake valve
Swirl number	Around 10

tight emission regulations.

The present work has previously been presented by the authors at the 2023 CIMAC conference [20].

2. Experimental setup

A modified 4-stroke, single cylinder Cooperative Fuel Research (CFR) engine, also used with ammonia in previous studies [6,7], has been significantly upgraded and used in present study (Fig. 1).

2.1. Engine geometries

The engine is an older CFR engine which originally had a limited compression ratio of 10. A 3D scan of similar CFR engine, performed by Argonne National Laboratory [21] is shown in Fig. 2. The compression ratio of the present engine has been raised to 15 by adding a disk on top of the original piston. This modification also added volume to the top land crevice, which is accounted for in the following analysis of crevice effects. The piston is shown in Fig. 3, where the blue colored part is the addition to the original piston.

The CFR engine has a side-mounted spark plug and a cutout is therefore made in the piston top to minimize any geometrical restriction for the flame to propagate from the spark into the main chamber. Previous studies of premixed methane on this specific engine showed that unburned fuel from top land crevice and ring pack is the major contribution to methane slip measured in the exhaust. This conclusion on methane slip from pre-mixed engines has also been made by other researchers [23,24]. Further support on this is currently being found by detailed CFD modelling to improve the understanding of flows and combustion patterns for this specific engine operated on pre-mixed methane [22]. These previous studies with pre-mixed methane combustion are mentioned here in context of pre-mixed ammonia combustion to emphasize that the slip of unburned fuel in both cases are highly determined by geometrical constraints for the specific engine.

In present study, the CFR engine had a shrouded intake valve installed, promoting swirl and turbulence in the combustion chamber.

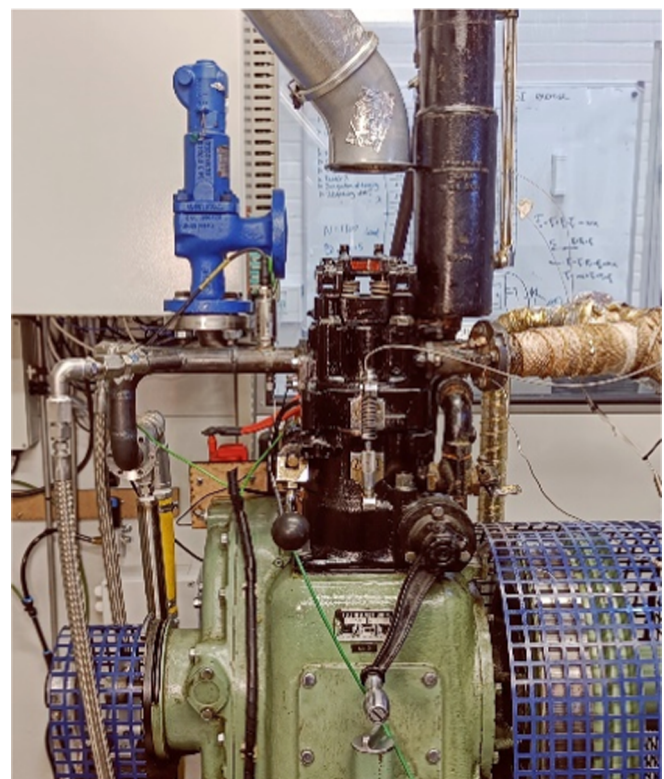


Fig. 4. CFR engine equipped with customized intake manifold for pre-mixed pressurized gas admission and back fire release valve.

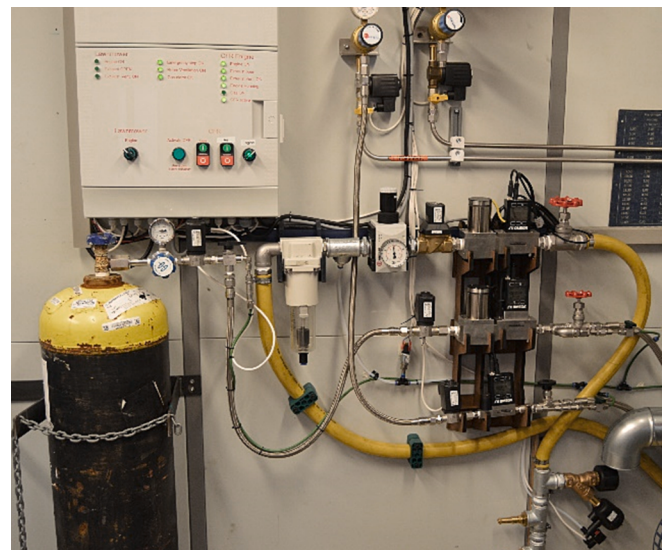


Fig. 5. Gas flow control system with safety measures to automatically shut down gas supply in case of leak detection or other failures.

The compression ratio and intake pressure were adjustable as specified in Table 1. Other geometrical specifications are similar to those reported in [6,7].

2.2. Engine gas controls

Significant upgrades have been made to improve the accuracy and adjustment range of gas control (Fig. 4 and Fig. 5), while all safety measures are integrated into the automatic control.

The air and fuel flows are adjusted with mass flow controllers

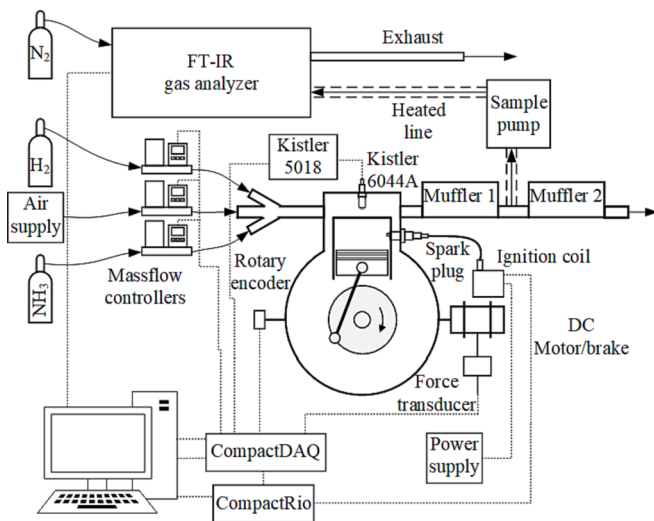


Fig. 6. Engine setup schematic.

Table 2
Specifications of ignition system used for the majority of presented engine tests.

Spark plugs	Denso VK20T Iridium+ 0.7–1.5 mm gap
Coil	MSD 8289 Smart Coil
Max energy	201 mJ at 10 ms dwell
Electrode diam.	0.4 mm

(Omega Engineering FMA 2600A) with a turn down ratio of 1:200 and a precision of \pm (0.8 % of reading +0.2 % of FS). The gases are mixed in the intake manifold 15 cm upstream of the intake port and assumed fully homogeneous in the combustion chamber due to mixing caused by the shrouded intake valve. This has previously been confirmed with a fast FID to measure the homogeneity of methane admitted to the engine.

The exhaust gas composition is analyzed using a MKS Multigas FTIR and the sample point is 5 m downstream from the engine after a mixer chamber insuring fully mixed exhaust gas. The exhaust pipe and mixing chamber is insulated and measurements are not made before the pipe wall is safely above the water condensation temperature. This is highly important when measuring exhaust gas from ammonia combustion, as any presence of condensed water will absorb unburned ammonia.

Pressure pulses in the exhaust system of a single cylinder engine have significant influence on the amount of trapped residual gas in the cylinder. In the current setup, the exhaust system is tuned to minimize the influence of the exhaust pulse at an engine speed of 1100 RPM.

Control of the engine and all data acquisition is performed with an in-house developed LabVIEW program. The cylinder pressure is measured with a Kistler 6044A pressure pick-up and a Kistler 5018 amplifier. The crankshaft position is measured with an optical encoder with 0.1 degree resolution. Both signals are acquired at a constant but high sample rate of 250 KHz and processed together to provide pressure data with highest possible angular resolution for every engine speed. All temperatures are measured with type-K thermocouples. A schematic overview of setup is shown in Fig. 6.

2.3. Ignition system

The engine is equipped with a smart ignition coil from MSD (8289 Smart Coil) with an integrated igniter circuit. This enables external control of spark timing and dwell time for the coil, which influences the spark discharge profile and ignition energy. A spark plug with an iridium center electrode and a platinum coated ground electrode is used to

Table 3
General structure of test matrix conducted in present work.

Test series	Investigating influence of	Ignition system	Compression ratio [-]	Air excess ratio [-]	P _{intake} [bar]	Spark timing
1	Ignition system	Varied	15	1 to lean misfire limit	1 and 1.3	Maximum Brake Torque
2	Compression temperature	TCI,	11 to 15	1.3	Varietd to get constant pressure at -30 CAD	-30 CAD
3	Compression pressure	5 ms dwell,	15		1 to 1.4	CA50 at 8 CAD
4	Air excess ratio	Ir + spark plug, 0.7 mm gap			1.2 and 1.4	
5	Intake pressure				1 to 1.3	
6	Combustion phasing					CA50 at -8 to 14 CAD

minimize electrode erosion during testing with sparks of longer duration (Table 2). In accordance with findings from the literature an effort was made to ensure that the available ignition energy would be sufficient for reliable combustion of neat ammonia/air mixtures. The MSD 8289 ignition coil delivers a stated 201 mJ of output energy at a dwell time of 10 ms, which should provide ample ignition energy according to previous findings. However, 5 ms dwell time (130 mJ) turned out to be sufficient and was used in this study if nothing else is specified. Other types of ignition systems and spark plugs have been tested but it is outside the scope to present here in detail.

2.4. Experimental procedure

Warm-up is performed until the oil temperature is at 60 °C and the exhaust sample location (coldest point in the exhaust) is above water condensation temperature. Mass flow controllers are tarred at zero flow before measurements are performed to ensure highest possible accuracy of fuel and air flows.

The spark timing is adjusted to provide 50 % heat release (CA50) at 8 CAD unless otherwise specified. This, rather than MBT (maximum break torque), is used as criteria for adjustment of spark timing because the torque varies weakly with spark timing compared to the emissions. CA50 at 8° CAD also provide MBT in most cases but is a more precise criteria to use, ensuring consistent emission trends for parameter sweeps of intake pressure, air excess ratio and compression ratios.

Motored pressure traces are recorded with warm engine for all compression ratios and intake pressures in extension of the corresponding fired tests on the same day.

The test campaign was organized to investigate the influence of key parameters by systematically changing them independently. The general structure of the test campaign is shown in Table 3 but during the campaign several tests were repeated on different days to check for repeatability and to ensure that there was no development of systematic error.

3. Data processing

All data processing is performed with in-house developed codes using Matlab and/or Python programming language. The Cantera toolbox [25] was used with gas property databases from Glarborg [19] for determination of chemical equilibrium and for looking up thermodynamic and transport properties of gases. The methodology behind the different cases of data processing is described in the following.

3.1. Pressure trace

The pressure in the combustion chamber is measured with a piezoelectric sensor. It is only providing the relative pressure trace and needs conversion to absolute pressure. The intake mass flow measurements are used to estimate the absolute pressure in the chamber and the influence of residual gas, by using an iterative procedure described in the following. This method applies only for engines with no valve overlap, which is the case with present CFR engine.

The total gas mass in the cylinder is considered as two separate volumes, the fresh charge of ammonia and air, and residual gas left from previous cycle. The pressure level in the cylinder is adjusted iteratively, until the total volume of fresh charge and the residual gas at IVC (intake valve closure), is the same as the geometrical volume at IVC. The volume of residual gas at IVC is determined with an isentropic process (eq. (3)) starting from the geometrical volume and the iterated pressure at EVC (exhaust valve closure).

$$V_{\text{residual@IVC}} = V_{\text{residual@EVC}} \cdot \left(\frac{P_{\text{EVC}}}{P_{\text{IVC}}} \right)^{\frac{1}{\gamma_{\text{exh}}}} \quad (3)$$

The heat capacity ratio is determined from the exhaust gas temperature

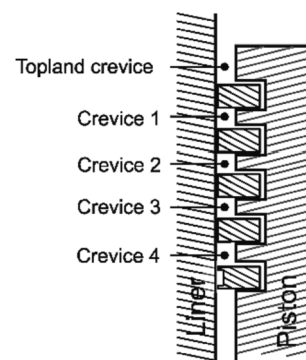


Fig. 7. Crevices of CFR engine.

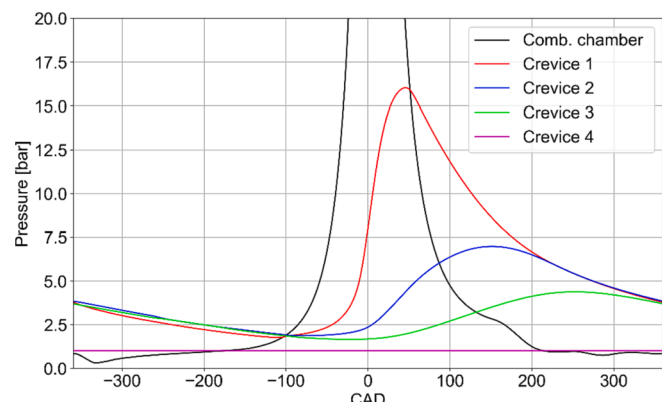


Fig. 8. Example of modelled pressure traces between piston rings as a result of measured pressure trace in the combustion chamber.

and composition.

The change of internal energy to the intake gas during the intake stroke is calculated from the piston pumping work (eq. (4)) subtracted the work required for the isentropic compression of the residual gas [26].

$$w_i = \int_{Ivo}^{IVC} P \cdot dv \quad (4)$$

By use of the intake temperature, the energy supplied as heat to the intake gas when it is passing the intake valve and the mass of intake gas, the trapped intake gas temperature and volume at IVC is calculated. The pressure is adjusted by iteration until the volume of residuals gas added with the volume of fresh intake gas matches the geometrical cylinder volume at IVC.

3.2. Heat release rate

The Heat Release Rate (HRR) is calculated using the first law of thermodynamics.

$$\dot{Q}_{AHR} = \frac{\gamma}{\gamma-1} p \frac{dV}{d\theta} + \frac{1}{\gamma-1} V \frac{dp}{d\theta} \quad (5)$$

where \dot{Q}_{AHR} is apparent heat release rate, γ is heat capacity ratio, p is cylinder pressure, V is cylinder volume, and θ is crank angle degree.

The non-reacting gas temperatures were calculated using step-wise isentropic process (eq. (6)) where the heat capacity ratio is an average between the T_1 and T_2 found by iteration.

$$T_2 = T_1 \cdot \left(\frac{P_2}{P_1} \right)^{\frac{1}{\gamma-1}} \quad (6)$$

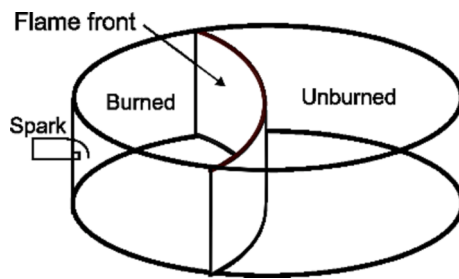


Fig. 9. Assumed flame development.

During combustion the cylinder volume is divided into a burned and an unburned volume. Unburned gas volume is converted to burned gas volume for every 10 % burned fuel, where the chemical equilibrium and temperature of burned gas is calculated. The heat capacity ratio used to calculate the apparent heat release rate during combustion is a weighted average of the burned and unburned volumes.

To correct for heat losses prior to combustion and to better identify the start of combustion, the HRR from a corresponding motored run is subtracted from the HRR of the fired case.

Integrating HRR is providing the heat release (HR), which is used to determine ignition delay, combustion phasing and combustion duration. The ignition delay is defined as the crank rotation from spark discharge to 10 % HR (CA10). Combustion phasing is defined as the crank position of 50 % HR (CA50). Combustion duration is defined as the crank rotation from 10 % HR (CA10) to 90 % HR (CA90). All data derived from the cylinder pressure is based the average of 50 consecutive cycles and the standard deviation of the data is illustrated in the following plots with error bars. The coefficient of variation (CoV) of indicated mean effective pressure (IMEP) is calculated by use of eq. (7), where $\bar{\text{IMEP}}$ is the mean IMEP and σ_{IMEP} the standard deviation of 50 consecutive cycles.

$$\text{CoV of IMEP \%} = \frac{\sigma_{\text{IMEP}}}{\bar{\text{IMEP}}} 100 \quad (7)$$

3.3. Crevice model

To calculate the amount of ammonia in the crevices, a previously in-house developed ring pack model is used. The model is based on [23,27]. An illustration of the crevices in the CFR engine is shown in Fig. 7.

The mass flows through ring gaps are assumed to be orifice flows and calculated by use of eq. (8). C_D is the discard coefficient set to 0.85 according to the work by Namazian [27].

$$\dot{m} = \eta \cdot C_D \cdot A \cdot \rho \cdot c \quad (8)$$

A is the ring gap area, ρ is the upstream density, c is speed of sound and η is the compressibility factor. Depending on the pressure ratio across the ring gap, this compressibility factor is calculated as either choked flow or subsonic flow according to the procedure described in [27]. The pressure development in each crevice is determined using conservation of mass and ideal gas law for each volume. An iteration procedure is used to obtain the equal pressure in crevices 1–3 at the end of the exhaust stroke. The pressure in crevice 4 is assumed to be atmospheric as in the crankcase, and mass entering crevice 4 is blow-by. An example of the pressure development between the rings derived with present model and a measured combustion pressure trace is shown in Fig. 8.

The state of the gases (burned versus unburned) entering the crevice is determined on basis of a simple flame propagation model and the measured combustion pressure trace. The model assumes a cylindrical shaped flame front, propagating radially from the side-mounted spark plug (Fig. 9). Using the instant location of the flame front in each time step, the fraction of burned/unburned gas entering the top-land crevice is calculated.

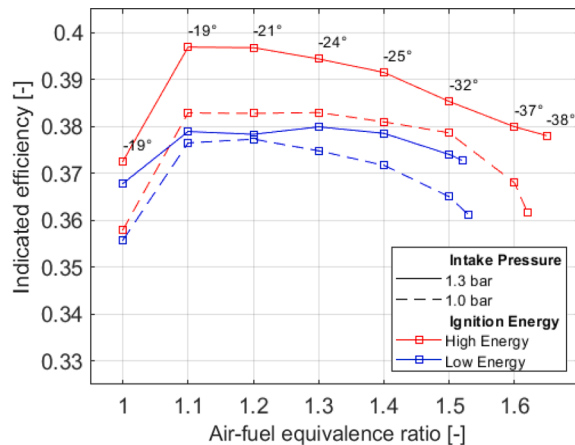


Fig. 10. Indicated efficiency from tests performed with TCI (Transistor Coil Ignition) system in both high and low energy setting and with Denso VK20T Iridium Plus 0.7 spark plug. The leanest engine operation in every series is measured at the Lean Misfire Limit (LML) defined here as CoV around 5 %. Spark timing is shown for selected points, only.

The gas temperature is assumed to adjust instantly to wall temperature after entry to the crevice. Unburned and burned gases are assumed to be fully mixed in the crevice. The exact dimensions of rings, gaps, grooves and crevice heights have been measured on the specific CFR engine used in the experiments.

3.4. FT-IR gas analysis

The concentration of individual species in a sample gas is quantified by fitting a composite spectrum, consisting of absorption spectra of individual species, to the measured absorption spectrum of the sample gas, using an in-house least squares (LSQ) routine.

To facilitate a full spectrum analysis, the residuals returned to the LSQ algorithm are weighted with the transmittance of the sample spectrum to the power of 2. This ensures that spectral regions with high absorption, i. e. low signal to noise, have little to no influence on the fitting procedure. The residual spectrum can be used to assess the quality of the fit and to identify potential species present in the sample, which are not included in the calibration database and thus the analysis.

Full spectrum analysis requires accurate calibrations of pure gases

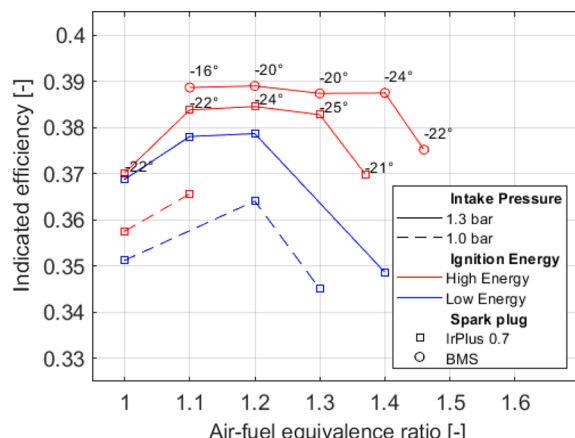


Fig. 11. Indicated efficiency from tests performed with CDI (Capacitive Discharge Ignition) system in both high and low energy setting with Denso VK20T Iridium Plus 0.7 spark plug and a Brisk DR08ZS Multi Spark Plug (BMS). The leanest engine operation in every series is measured at the Lean Misfire Limit (LML) defined here as CoV around 5 %. Spark timing is shown for selected points, only.

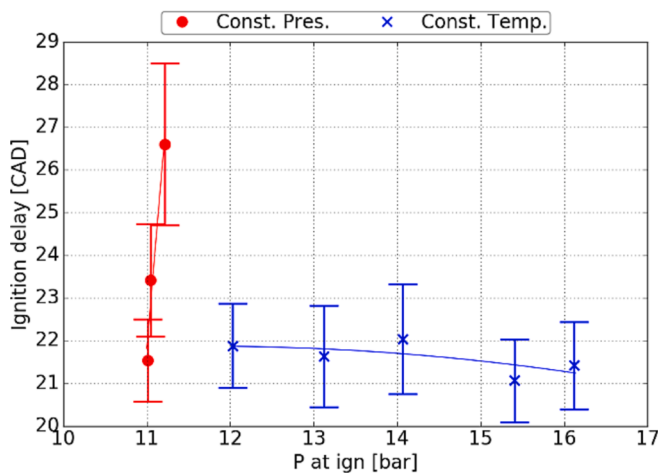


Fig. 12. Ignition delay against pressure at -30 CAD showing that gas pressure has a weak influence on ignition delay if the gas temperature is kept constant.

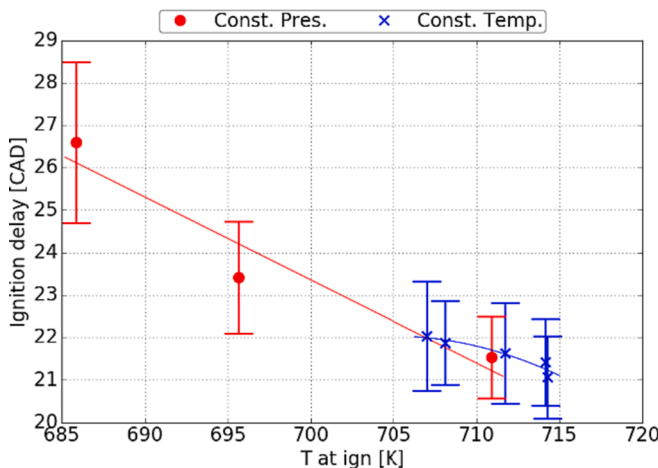


Fig. 13. Ignition delay against temperature at 30 CAD showing that gas temperature has a strong influence on ignition delay even if the gas pressure is kept constant.

diluted in pure nitrogen at known concentrations in the whole range of interests. Calibration spectra have been made in-house using certified calibration gases and a certified HovaGas G6 gas mixer to produce gas concentrations of an accuracy around 2 % standard deviation for the whole concentration range of relevance for the engine measurements.

4. Results and discussion

A large range of experiments have been conducted to investigate the limits and explore optimal engine operating conditions for neat ammonia combustion. Four key parameters have been identified to be most critical in the assessment of premixed ammonia combustion.

- Indicated efficiency should be high to minimize fuel consumption.
- CoV (Coefficient of variation) of IMEP (Indicated Mean Effective Pressure) should be low to ensure smooth engine operation and stable exhaust composition.
- NH₃/NO_x molar ratio in the exhaust composition should be close to 1 to enable complete conversion of both unburned ammonia and NO_x in a SCR catalyst.
- N₂O should be as low as possible, preferably zero, as it is a strong greenhouse gas. The global warming from use of green ammonia may

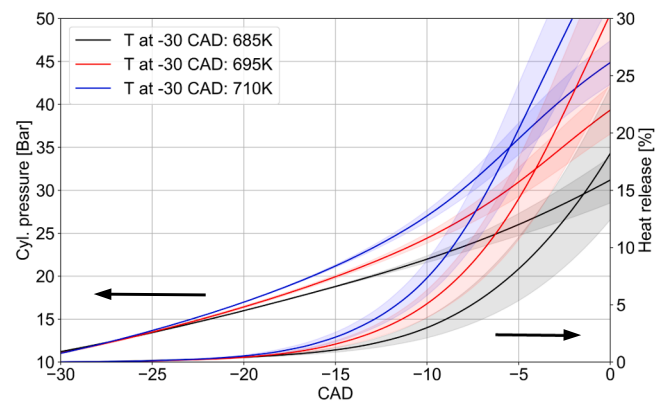


Fig. 14. Heat release for constant pressure and varied temperature at -30 CAD (spark timing).

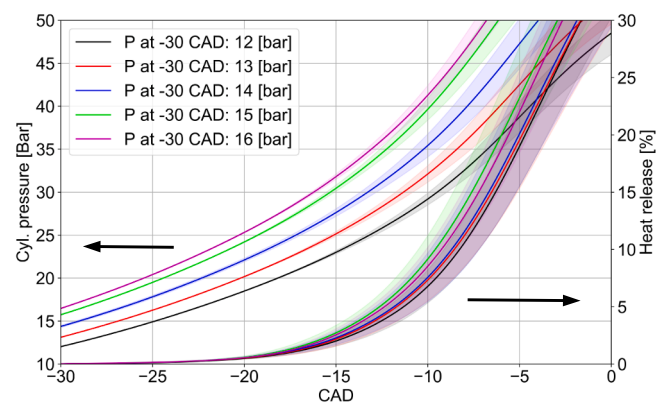


Fig. 15. Heat release for constant temperature and varied pressure at -30 CAD (spark timing).

actually become higher than from fossil diesel if concentrations of N₂O is too high.

These key parameters and the tradeoffs are analyzed and discussed in the results.

4.1. Ignition tests

Initial testing with the ammonia fueled SI engine indicated that satisfactory engine operation was possible with the right type of spark discharge and spark plug. An air excess ratio of 1.5–1.6 was attainable with reasonably low CoV. Two different high energy ignition systems were tested during the preliminary experiments, a CDI (Capacitive Discharge Ignition) system and a TCI (Transistor Coil Ignition) system. The CDI system is characterized by a short and powerful discharge of energy stored in capacitors, while the TCI system relies on the inductance of coils with primary and secondary circuits to store and release

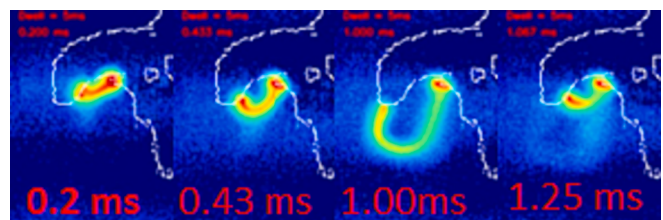


Fig. 16. High speed imaging of high energy spark exposed to 8 m/s air flow at atmospheric pressure.

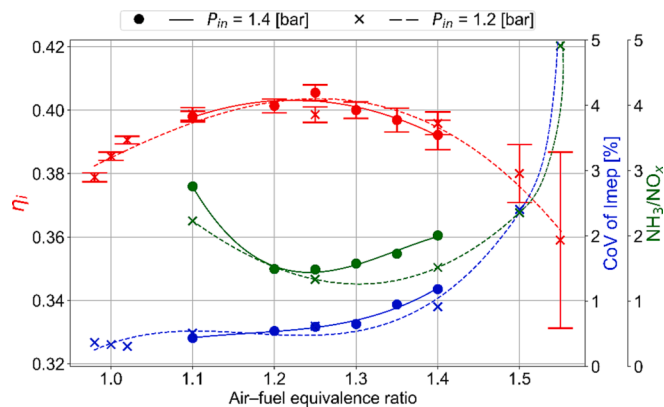


Fig. 17. Performance with varied air excess ratios for two intake pressures.

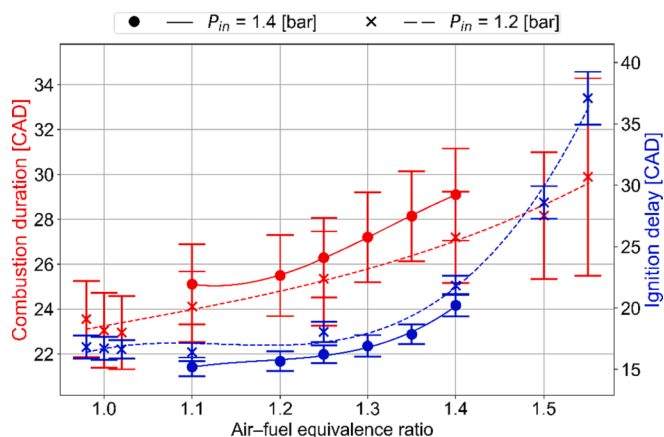


Fig. 18. Combustion duration and ignition delay for varied air excess ratios and two different intake pressures.

energy via the spark plug. With the inductive TCI system, stable engine operation was achievable for a wider range of spark timings compared to the CDI system, where combustion stability was very sensitive to spark plug choice and spark timing. It was possible to take advantage of the high octane rating of ammonia by increasing intake pressure, which extended the LML (Lean Misfire Limit) defined as CoV of IMEP > 5 %. Increasing intake pressure demands higher voltage from the ignition coil because the breakdown voltage required for an arc to be formed increases with cylinder pressure. With increased intake pressure the spark timing should also be retarded to maintain the desired CA50 value for the shorter ignition delay. This increases the breakdown voltage even further. It was affirmed that lean operation is sensitive to ignition coil dwell, spark plug type, electrode gap, and resistance in spark plug and ignition leads. The most extreme combinations of high spark energy, a large electrode gap and late spark timing significantly increased electromagnetic interference with the sensitive electronics and caused troubles with the engine controls. However, it proved possible to find compromises for reliable ignition of lean air/ammonia mixtures up to $\lambda \approx 1.66$ before CoV exceeded 5 % (Fig. 10 and Fig. 11).

It should be noted that the results shown in Fig. 10 and Fig. 11 are from an early state in the test campaign where MBT was used as criteria for optimum spark timing rather than CA50 at 8 CAD which was used as criteria in most of the presented work.

The influences of gas temperature and pressure on ignition delay was further investigated using the TCI ignition system with a fixed dwell time. Spark timing was kept fixed at -30 CAD while gas temperature and pressure at -30 CAD was varied independently. By only changing the intake pressure, an almost constant temperature at different pressures was maintained at -30 CAD. By changing compression ratio and

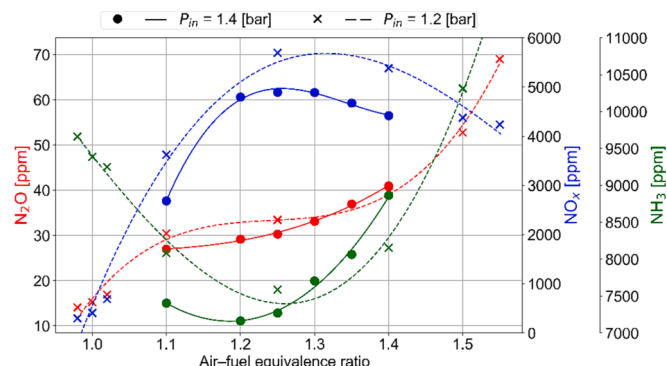


Fig. 19. Measured NH₃, NO_x and N₂O concentrations for varied air excess ratios and two intake pressures-NH₃ concentration at $\lambda = 1.55$ is not shown but is measured to be around 20800 ppm.

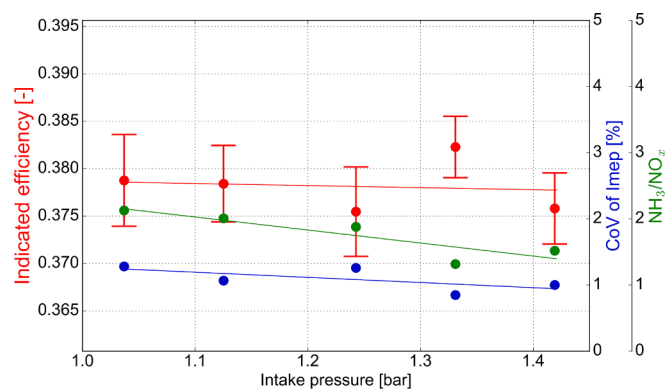


Fig. 20. Performance with varied intake pressure and fixed air excess ratio.

adjusting the intake pressure to maintain a constant pressure at -30 CAD only the temperature was varied.

It is seen that increasing pressure has a weak influence on the ignition delay (Fig. 12), whereas temperatures of the mixture have a strong influence on the ignition delay (Fig. 13). These findings will depend slightly on how ignition delay is defined. In this work, ignition is defined as CA10 (10 % heat release) which is commonly used. Fig. 14 and Fig. 15 shows the measured cylinder pressure and relative heat release, where it is evident that temperature has a significantly larger influence on ignition delay than pressure, regardless of how ignition is defined.

Voltage in the ignition lead was measured with a capacitive high voltage probe and sampled with a PicoScope 2405A oscilloscope. These measurements indicated that the spark did not have a smooth glow phase in the final stage of the spark discharge if the spark was set to jump in parts of the engine cycle with high swirling flow. To understand this further, a small series of high-speed imaging of the spark was recorded at atmospheric pressure with a constant air flow of approximately 8 m/s near the spark gap (Fig. 16). This showed that the spark is re-striking several times. The number of possible re-strokes is strongly influenced by the dwell time of the coil. This interaction between swirling flow and a spark that is strong enough to stretch and re-strike several times during a single discharge event is believed to be a key ingredient in successful ignition of neat ammonia. A more detailed investigation on this topic is in preparation by the authors.

4.2. Influence of air excess ratio

The influence of air excess ratio on indicated efficiency, CoV and emissions has been investigated to find the optimal operation range for premixed ammonia combustion.

The results in Fig. 17 show that optimum efficiency, minimum CoV

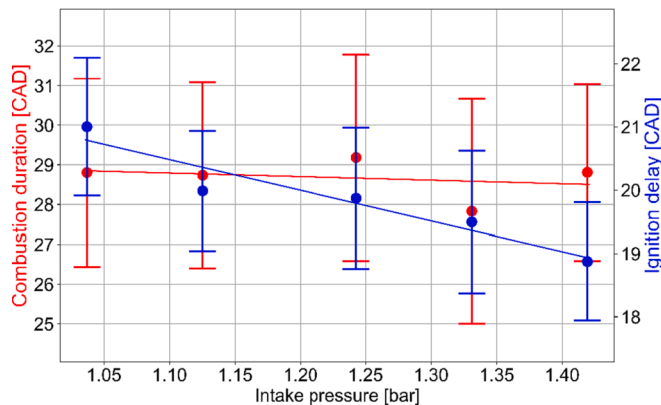


Fig. 21. Combustion duration and ignition delay for varied intake pressure and fixed air excess ratio.

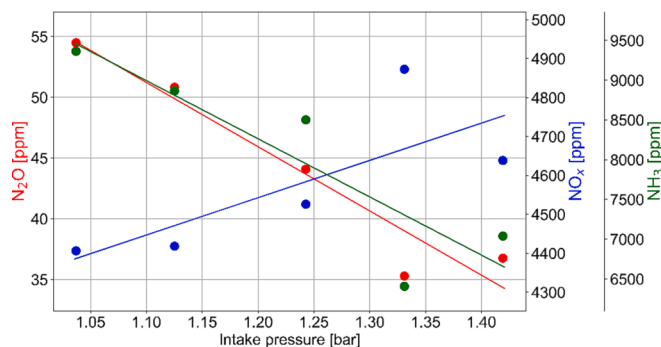


Fig. 22. Measured NH_3 , NO_x and N_2O concentrations for varied intake pressure and fixed air excess ratio.

and NH_3/NO_x ratio coincide at an air excess ratio around $\lambda = 1.25$. This trend seems not to depend significantly on the intake pressure. The results also suggest that a rather wide range of air excess ratios could be tolerated for short periods of time, which may be critical in transient engine operation where the air excess ratio may fluctuate during load adjustments.

The combustion duration and ignition delay are both increasing with air excess ratio (Fig. 18) as flame speeds decrease and required ignition energy increases.

It should be noted that the ignition delay and combustion duration in Fig. 18 deviates from some of the other measurements. Particularly at intake pressure 1.2 bar they are longer than usual. The indicated efficiency in Fig. 17 is also slightly higher than usual. Those sweeps of air excess ratio were performed early in the test campaign and the valve gap was slightly out of adjustment during these tests. It was readjusted before the test campaign continued. It has come as surprised that this small adjustment seems to have such an impact to the results. A larger expansion ratio and a different scavenging efficiency caused by the slightly larger valve gap is the only explanation to find, which certainly will have to be investigated further in future work. However, the conclusions that can be drawn from the observed trends are still considered to be valid.

The N_2O concentration is lowest close to stoichiometric mixture whereas the NH_3 slip is high and the NO_x concentration is low (Fig. 19). This is also reflected in the large NH_3/NO_x ratio in Fig. 17. With the current methods of after treatment systems it will probably be a better compromise to accept 2–3 times higher N_2O and operate the engine around $\lambda = 1.25$ where the NH_3/NO_x ratio is closest to 1.

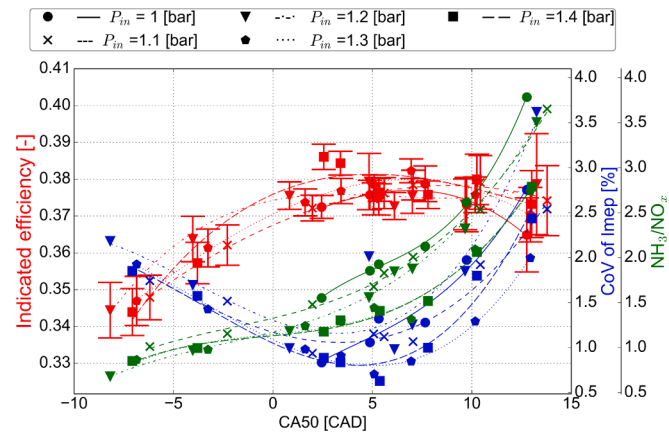


Fig. 23. Performance with varied combustion phasing for several intake pressures and fixed air excess ratio.

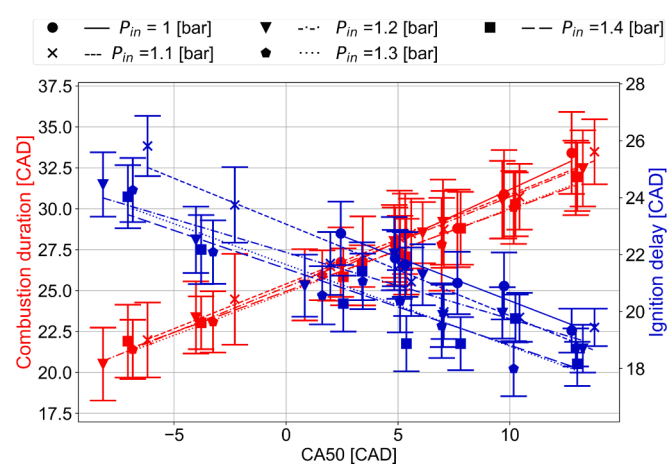


Fig. 24. Combustion duration and ignition delay for varied combustion phasing at several intake pressures and fixed air excess ratio.

4.3. Influence of intake pressure

In the following series of measurements, the engine was operated at a fixed air excess ratio of 1.31 ± 0.04 . In hindsight, $\lambda = 1.25$ would have been a better choice according to above analysis but the measurements were performed before a detailed analysis was made. However, $\lambda = 1.31$ is considered close enough to the optimum air excess ratio to draw valid conclusions from the following parameter sweeps.

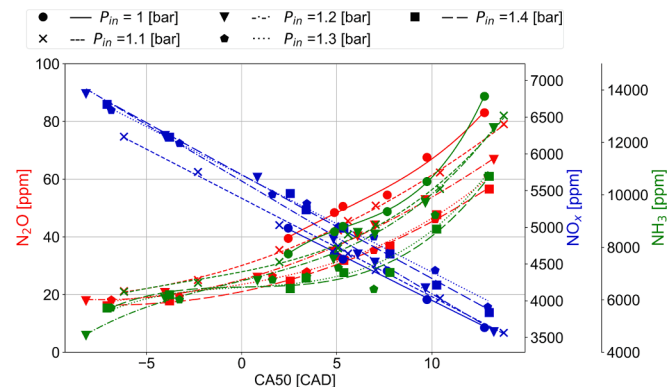


Fig. 25. Measured NH_3 , NO_x and N_2O concentrations for varied combustion phasing with several intake pressures and fixed air excess ratio.

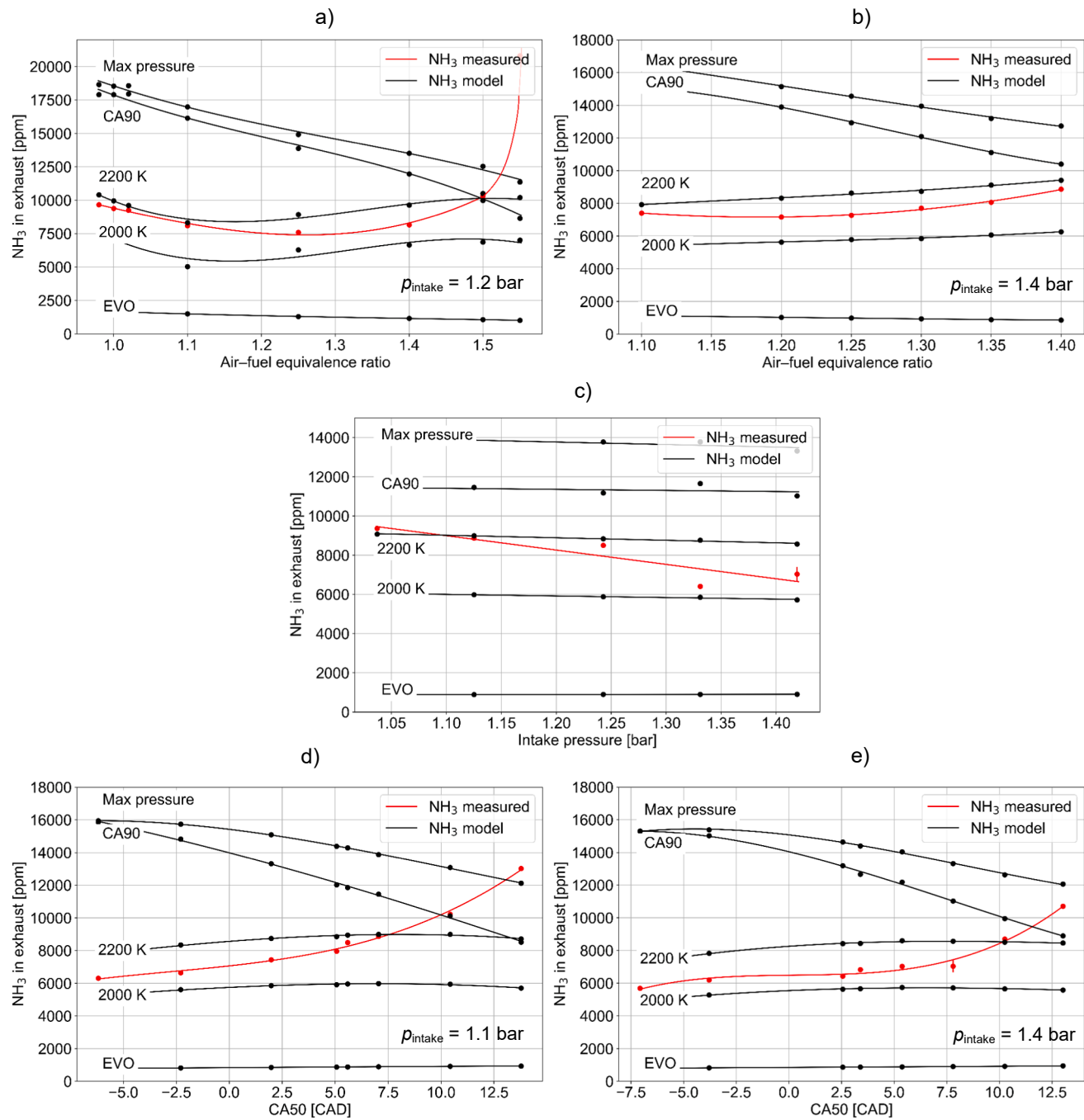


Fig. 26. Collection of calculated (black) NH_3 concentrations in the exhaust gas if post-oxidation is stopping to occur at indicated bulk gas temperatures of burned gas (2000 K or 2200 K) or at indicated events in the expansion stroke (CA90 or EVO). The red curve show NH_3 concentrations measured for the different parameter sweeps. (For interpretation of the references to colour in this figure legend, the reader is referred to the web version of this article.)

The indicated efficiency and CoV is rather constant for the whole range of investigated intake pressures and air excess ratio held constant (Fig. 20). This is a promising result toward increasing the break thermal efficiency of an ammonia engine by further increasing the charge pressure to downsize the engine and minimize the mechanical losses. An even more promising result shown in Fig. 20 is that the NH_3/NO_x ratio approaches unity toward the higher intake pressure, suggesting that at least at high load, it should be possible to reduce both NH_3 and NO_x in an SCR reactor.

The combustion duration shown in Fig. 21 is not significantly influenced by the intake pressure, which supports the constant indicated efficiency observed in Fig. 20.

However, the ignition delay decreases slightly with increasing intake pressure in Fig. 21, which seem to contradict with the findings in Fig. 12. Here it should be reminded that the measurements in Fig. 21 were performed with spark timing adjusted to CA50 at 8 CAD and not a fixed spark timing as in Fig. 12.

The weak dependency of ignition delay on intake pressure and the independent combustion duration shown in Fig. 21 suggests good adaptability to fast load variations in transient engine operation.

Fig. 22 shows that the influence of intake pressures on the NH_3/NO_x ratio in Fig. 20 is due to a significant reduction of NH_3 and a weak increase of NO_x with increasing intake pressure. The N_2O concentration is reduced along with NH_3 when intake pressure is increased.

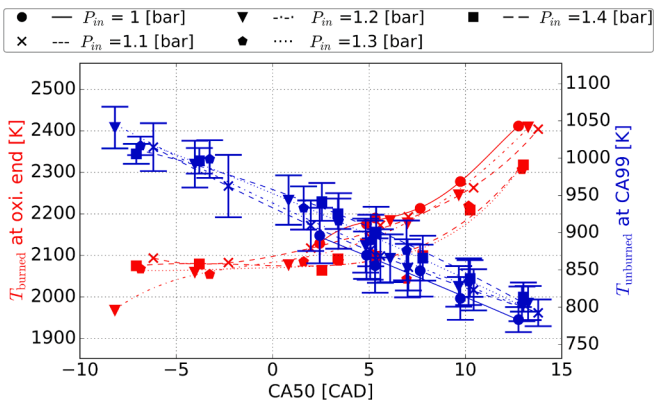


Fig. 27. Plot burned gas temperatures at which post-oxidation should stop to occur to match the measured NH₃ concentration in the exhaust gas for all tests performed with $\lambda = 1.31 \pm 0.04$. Also shown is the unburned gas temperature of end gases at the end of heat release (CA99).

4.4. Influence of combustion phasing

Early in the experimental campaign it became evident the combusting phasing has a large influence on emissions. To investigate this fully and to verify the consistency of trends, a rather comprehensive series of tests was made with ignition sweeps for a wider range of intake pressures.

It is evident from Fig. 23 that using CA50 at 8 CAD rather than MBT timing in the test campaign has been a good choice. The actual crank position of MBT (where indicated efficiency is at maximum) is rather consistently occurring with CA50 between 5 and 8 CAD. In terms of CoV a better compromise for future work would be to use CA50 at 5 CAD. When harder compromises have to be made in order to comply with emission regulations it seems beneficial with even earlier combustion phasing as the NH₃/NO_x ratio approaches unity.

The performance trends observed in Fig. 23 are very consistent and almost coinciding for all investigated intake pressures. This is also the case for ignition delay and combustion duration shown in Fig. 24. It is no surprise that the ignition delay is longer when earlier spark timing is required for advancing combustion phasing and it is also no surprise that the combustion duration is shorter when the combustion phasing is advanced. It is however a surprise how consistent the combustion behaves across the range of intake pressures compared to more traditional fuels. The most likely reason for this is the low ignitability of ammonia causing ignition delay and end gas combustion to be rather insensitive to indirect changes, such as wall temperatures and residual gas amounts when intake pressure is changed. Thus, with a proper ignition system, the low ignitability of ammonia actually offers maximum control of the combustion phasing with predictable behavior across various load conditions.

It is also a positive surprise that compromising the combustion phasing to favor a NH₃/NO_x ratio close to unity also favors lower N₂O emissions (Fig. 25).

Fig. 25 shows that NH₃ and N₂O concentrations are strongly correlated as Fig. 19 and Fig. 22 also showed for the other parameter sweeps. NH₃ and N₂O concentrations stagnate toward the earliest combustion phasing with a N₂O level around 20 ppm. NO_x continues to increase toward earlier combustion phasing which offers continued control of the NH₃/NO_x ratio by adjustment of the spark timing.

4.5. Influence of engine crevices

For the present engine, with seemingly good combustion process, it is the hypotheses that unburned ammonia in the exhaust almost exclusively originates from crevice releases. Experiments performed by the authors with lean pre-mixed methane, on the exact same test setup,

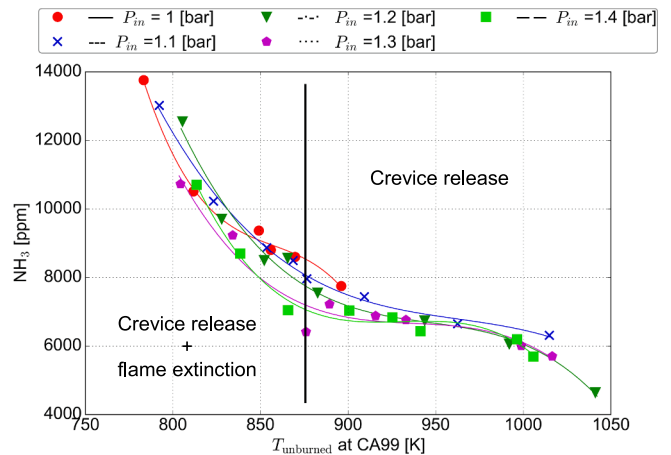


Fig. 28. Measured NH₃ concentrations of all tests performed with $\lambda = 1.31 \pm 0.04$ against the unburned gas temperature at the end of heat release (CA99).

support this hypothesis. With methane operation a fast FID (Flame Ionization Detector) made it possible to measure instantaneous concentration of hydrocarbon in the exhaust streaming through the exhaust port during exhaust stroke. These investigations, yet to be published, showed that hardly any hydrocarbons could be detected during release of the bulk combustion gas but high concentrations were released late in the expansion stroke where crevice gases are released. The indicated efficiency with operation on ammonia and optimum spark timing is slightly higher than that measured with methane and therefore suggests that there should not be significant quenching or incomplete combustion of bulk gas in the ammonia case either.

To further test this hypothesis, the earlier described crevice model is used to determine how much ammonia is trapped in the ring and piston top-land crevices at every CAD during the expansion, based on the measured pressure traces. The ammonia released from the crevices can be converted into concentrations that would be present in the exhaust gas if it escapes without reacting. The challenge is to determine when post oxidation of the crevice releases will stop to occur during the expansion stroke.

The simple approach used here for testing the hypothesis, is to plot calculated ammonia concentrations in the exhaust gas as result of crevice release if post-oxidation stops to occur at different burned bulk gas temperatures. These curves are plotted together with measured ammonia concentrations in the exhaust gas for a wide range of parameter sweeps (Fig. 26).

The results of this analysis seem to support the hypothesis and suggest that post-oxidation stop to occur when the released crevice gases are mixed into a burned bulk gas colder than 2100 K.

However, there are deviations from the hypothesis that need to be understood. Particularly, when NH₃ concentration measured in the exhaust is exceeding the largest possible crevice release that would occur if the whole release from maximum combustion pressure to EVC escaped non-reacted.

At the leanest operation with 1.2 bar intake pressure in Fig. 26 a), this deviation is most likely due to the proximity to the lean mixture limit where pockets of premixed gas did not have enough time to burn completely before expansion.

With varied intake pressure in Fig. 26 c) the bulk gas temperature at which post-oxidation stop to occur is slightly decreasing toward higher intake pressures. This trend is likely caused by the larger thermal load on cylinder and piston surfaces when intake pressure and thus load is increased. The temperature of the crevice gas is assumed to adjust to the crevice wall temperature and if the gas is released with a higher temperature it will require less heat from the bulk gas to enable post-oxidation.

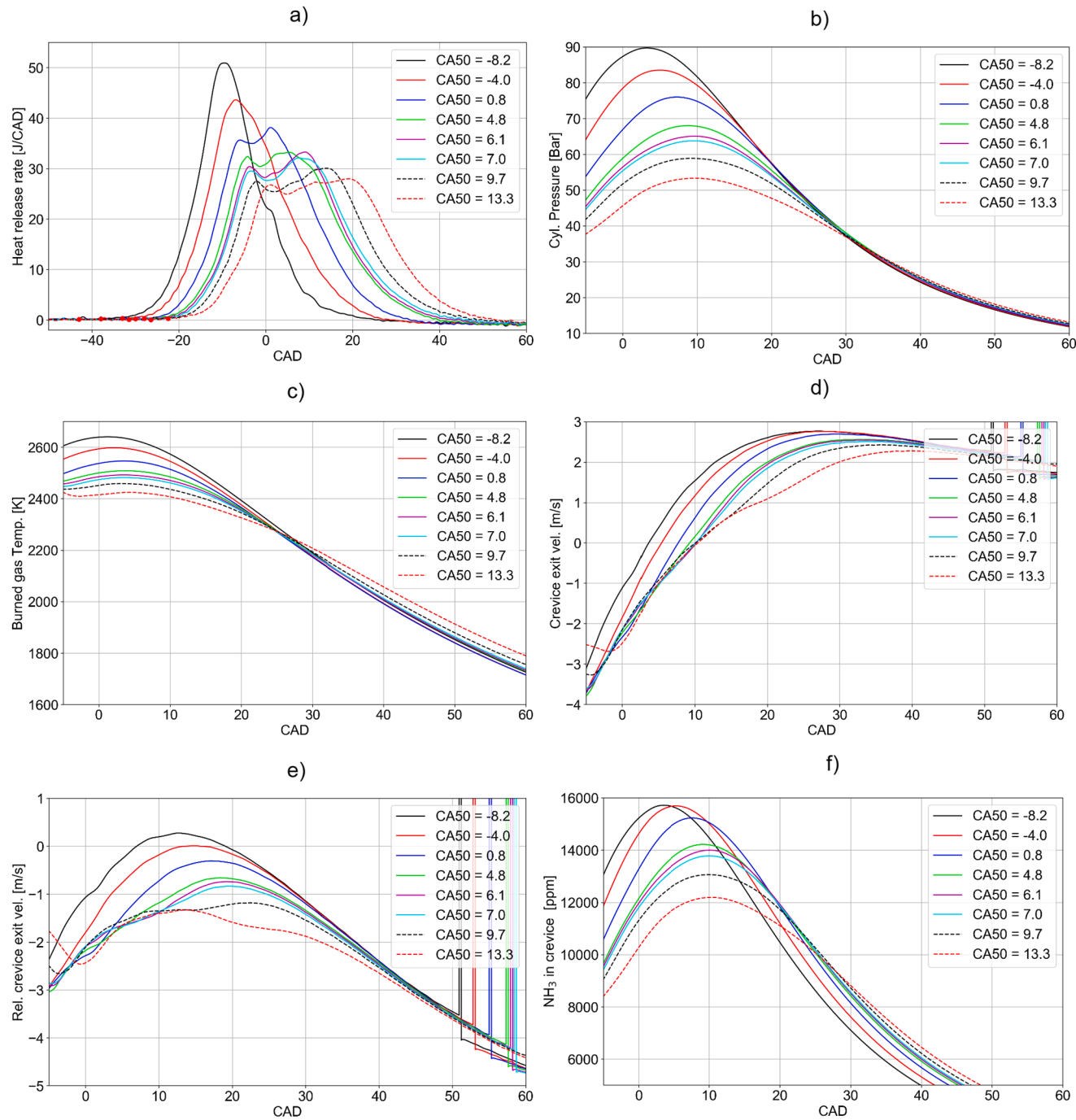


Fig. 29. Detailed plots of calculated crevice releases for different combustion phasing of measurements with 1.2 bar intake pressure and $\lambda = 1.31 \pm 0.04$.

It is harder to understand why it should require higher burned gas temperature to enable post-oxidation of crevice releases with late combustion phasing shown in Fig. 26 d) and e). To verify the consistency of this trend, the lowest bulk gas temperature required to match the non-reacted NH₃ releases from crevices with measured NH₃ concentration in exhaust gas was determined and shown in a single plot for combustion phasing sweeps of all intake pressures (Fig. 27).

Fig. 27 shows that trends are consistent for all loads and it also shows good constancy of unburned gas temperature at the very end of the measured heat release (CA99). The unburned temperature is determined from measured pressure traces and measured inlet mass flow of air and fuel with the treatment of residual gas as described in section 3.1. It does not seem likely that it should require a higher burned bulk gas

temperature to enable post-oxidation of crevice releases when combustion phasing (CA50) is adjusted later than 5 CAD as indicated in Fig. 27. It is more likely that flame extinction starts to occur with late combustion phasing and contributes to the total NH₃ slip and as indicated by Fig. 27 this should start to occur when the temperature of unburned gas drops below the 850–900 K range. This also seems evident from the raw NH₃ measurements plotted against the unburned gas temperature at CA99, shown in Fig. 28.

Further evidence is found in the more detailed plots of heat release rates, burned gas temperature and unburned gas left in the crevice. Heat release ends around 40 CAD for those cases with late combustion phasing (Fig. 29 a) and that is also where the burned gas temperature drops below 2100 K (Fig. 29 c). However, there is only NH₃ left in the

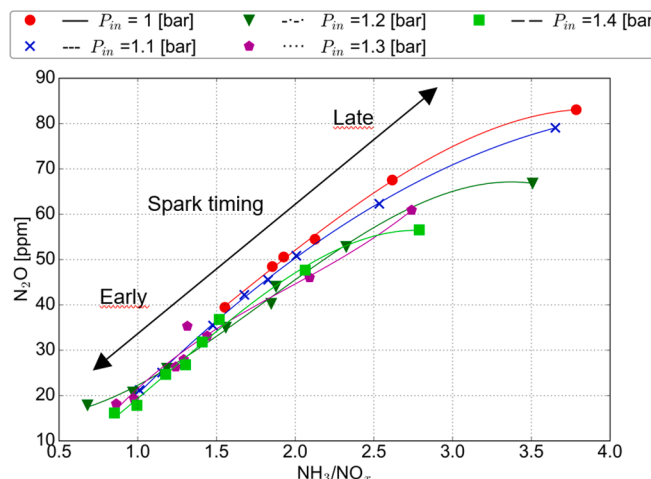


Fig. 30. N_2O vs- NH_3/NO_x ratio with $\lambda = 1.31 \pm 0.04$ and different spark timings.

crevice to account for around 6000 ppm NH_3 in the exhaust (Fig. 29 f) which is only 50–70 % of the measured NH_3 slip (Fig. 25).

The detailed plots in Fig. 29 also helps to better understand why the NH_3 slip is so systematically reduced with combustion phasing earlier than 5 CAD where flame extinction do not seem to occur. It is expected that the combustion pressure is higher with earlier combustion phasing and that pressure and burned gas temperature will converge toward similar levels as the expansion of burned gasses also start earlier (Fig. 29 b and c). It is however surprising that unburned fuel contained in the crevices is significantly reduced with early combustion phasing despite the fact that it contains more gas because of the higher combustion pressure (Fig. 29 f). The reason for this is that the crevice model take into account that the gas entering the crevice is either unburned or burned gas depending on the location relative to the propagating flame front. Thus in the present engine with side mounted spark plug, it will be burned gas entering the crevice close to the spark plug soon after start of combustion. The current flame propagation model is assuming radial propagation from the spark plug with a flame speed determined from the measured heat release rate. The model do not account for swirl and other large structures in the gas flow. However, the model seems to capture the measured trends despite this simplification. A detailed CFD model is currently under development for this exact same engine to investigate the influence of swirl and crevice releases [22].

Another feature of early combustion phasing is the higher exit velocity of crevice gas during the early expansion. A larger amount of NH_3 is trapped with early combustion phasing but it is quickly released and with a higher exit velocity that improves mixing with hot combustion products and the chance for complete post-oxidation is improved. Particularly if the exit velocity relative to the piston velocity is high this mixing will be improved. The crevice release is more likely to stick to the cold liner wall when the piston moves downward if the exit velocity, relative to the wall, is low. The relative exit velocity is higher early in the expansion stroke due to the lower piston velocity. Estimated exit velocity and relative velocity is also shown in Fig. 29 d) and e). The model assumes a uniform velocity distribution along the peripheral exit area defined by the clearance between liner and piston top land. In reality there will be a local jet of higher velocity at the exit above the ring gap of the top piston ring. The influence of this is also being investigated further with the more detailed CFD model under development [22]. The large steps seen in the plots of crevice exit velocities around 50–60 CAD in Fig. 29 d) and e) is caused by a directional shift of pressure forces acting on the top ring causing it to move and seal against the upper land in the ring groove.

4.6. N_2O

Emission measurements throughout the campaign have shown a strong correlation between N_2O and NH_3 emissions and importantly in terms of SCR application, this trend is maintained with a systematically lowering of N_2O as NH_3/NO_x approaches unity (Fig. 30).

This systematic relation also suggests that N_2O formation is dominated by the crevice mechanism. As N_2O is an intermediate species formed at intermediate temperatures it will inevitably be formed at some point in time during the expansion stroke where a transition from complete oxidation of crevice release to a non-reacting release happens. Experiments with late combustion phasing deviates from the general trend which is likely due to flame extinction causing the crevice mechanism to not be the only mechanism responsible for NH_3 slip and N_2O formation.

A promising feature about the linear relation, shown in Fig. 30, is that it may be possible to use a fast responding closed loop control system to adjust the spark timing based on signals from NO_x and NH_3 sensors located after a SCR catalyst. This will be quite similar to the control system ensuring stoichiometric combustion for the 3-way catalysts in gasoline cars using a closed loop control system on the signal from a lambda sensor to adjust fuel injection. An adaptive adjustment of spark timing on the present engine would at the same time ensure lowest possible N_2O emission assuming N_2O formation in the SCR catalyst can be omitted.

5. Marine engine considerations

The present test engine is a spark ignited 4-stroke engine but actually it has more similarities with pre-mixed dual fuel types of 2-stroke marine engines than with the 4-stroke counterpart in some aspects. This has turned out to be particularly important for ammonia combustion.

Similarities are that 2-stroke marine engines has a centrally located exhaust valve with pilot fuel injected tangentially in the periphery of a strong swirling gas flow on top of rather flat piston. The CFR engine used in present experiments also has a rather flat piston top, a strong gas swirl due to the shrouded valve and the spark plug is side mounted. The 4-stroke marine engines typically have 4 valves and an injector in the center of the fire deck. Pilot fuel is injected radially into a bowl in the piston with rather quiescent air. This means that conditions where the premixed gas charge is ignited in the periphery of a strong swirl and burning toward the center can be more easily be obtain in both the CFR engine and the pre-mixed 2-stroke marine engines. Whereas the pre-mixed charge in traditional 4-stroke engines is burning in direction from the bowl toward the periphery of the chamber through a rather cold squish volume where crevice volumes are released.

The leanings obtained from present study with a premixed charge of pure ammonia and air is that proper managing of crevice volumes is the key to handle emissions. One method to do this is to initiate combustion close to the crevice entrance to reduce the amount of unburned ammonia squeezed into the ring crevices during combustion. Another method is to reduce crevice volumes. This suggest that the geometry and flow conditions in a pre-mixed 2-stroke marine engine will be better suited for premixed ammonia combustion in a dual fuel, pre-mixed ammonia and diesel spray concept. The bowl configuration required for good diesel combustion in typical 4-stroke engines will be less suited for premixed ammonia combustion due to the large squish volume that will be quenched and squeezed into the ring crevice.

A dedicated 4-stroke engine for premixed ammonia with better emission performance than in the present study could certainly be developed. However, it may be difficult to obtain good performance on only diesel with that same engine because of its need for a bowl.

It is uncertain if the same level of stable ignition, fast combustion and composition of emissions obtained in present study would also be achieved if the spark was replaced with a diesel spray. However, it seems unlikely that the performance should become better by using a diesel

spray as ignition source. Thus, it is believed that the present study serve as a best case scenario to investigate the crevice effects that will also be present if another ignition source is used.

In more general, present experiments suggest that higher charge pressure than possible in present study will improve brake thermal efficiency and reduce emissions. Higher compression ratio than possible in present study will most probably also improve efficiency but slightly increase emissions. However, pre-ignition and knocking will definitely not be a limiting factor. Preliminary experiments showed that lowering the engine speed had no significant influence on N₂O emissions. Thus, lower engine speed and larger engine dimensions should only improve the possibility to reduce the relative size of crevice volumes and emissions even further. The break thermal efficiency has also potential to become higher than with diesel operation particularly because high NO_x levels are actually desired in order to reduce the ammonia slip but also because pressure rise rates can be kept under control due the combustion properties of ammonia.

6. Conclusion

Successful ignition of neat ammonia at lean condition can be achieved using excessive energy charging of an inductive spark ignition system. Excess charge allow the arc to stretch longer and move along with the swirling flow in the CFR engine before it collapses and restrikes several times during a single spark event.

The optimal air-fuel equivalence ratio was found to be 1.25. At this air excess an optimum indicated efficiency, low CoV and low NH₃/NO_x ratio close to unity was found. Increasing the intake pressure reduces the NH₃/NO_x ratio and lower the N₂O as well. With the present engine, final adjustment to obtain a NH₃/NO_x ratio of unity and minimum N₂O emission was made by advancing the spark timing and compromising the engine efficiency slightly. A NH₃/NO_x ratio of unity and minimum N₂O emission are critical criteria's for NH₃ operation of engines in order to achieve complete NH₃ and NO_x removal with an SCR catalyst and minimize global warming from N₂O.

The investigation provides evidence that ammonia slip from the present engine primarily originates from unburned fuel trapped in crevices during combustion, and released during the expansion. There is also evidence that N₂O is formed during a part of the expansion stroke when crevice releases are mixed with burned gas just hot enough for partly oxidation of NH₃. The present test engine has a rather large crevice volume relative to combustion chamber. A smaller crevice would lower the slip of ammonia and this would also lower the N₂O emission as well as the NH₃/NO_x ratio because the NO_x would not be affected by the smaller crevices volumes.

Declaration of Competing Interest

The authors declare that they have no known competing financial interests or personal relationships that could have appeared to influence the work reported in this paper.

Data availability

Data will be made available on request.

Acknowledgments

The ammonia ignition investigations are performed as part of the project “AEngine - Zero-Carbon Ammonia Marine Engine” financially supported by Innovation Fund Denmark (IFD) and emissions investigations are performed as part of “Engimmonia - Sustainable technologies for future long distance shipping towards complete decarbonisation” financially supported by European Union’s Horizon 2020 research and innovation program under grant agreement n° 955413.

Appendix A. Supplementary material

Supplementary data to this article can be found online at <https://doi.org/10.1016/j.fuel.2023.130159>.

References

- [1] Thomas G, Parks G. Potential Roles of Ammonia in a Hydrogen Economy - A Study of Issues Related to the Use Ammonia for On-Board Vehicular Hydrogen Storage. U. S. Department of Energy; 2006.
- [2] Klüssmann JN, Eknud LR, Ivarsson A, Schramm J. Ammonia Application in IC Engines - A literature review. IEA-AMF Special Report; 2020.
- [3] Cornelius W, Huellmantel LW, Mitchell HR. Ammonia as an Engine Fuel. SAE Technical Paper 1965;650052. <https://doi.org/10.4271/650052>.
- [4] Pearall TJ, Garabedian CG. Combustion of anhydrous ammonia in diesel engines. SAE Technical Paper 1967;670947. <https://doi.org/10.4271/670947>.
- [5] Gray JT, Dimitroff E, Meckel NT, Quillian RD. Ammonia fuel - engine compatibility and combustion. SAE Technical Paper 1966;660156. <https://doi.org/10.4271/660156>.
- [6] Mørch CS, Bjerre A, Gøttrup MP, Sorenson SC, Schramm J. Ammonia/hydrogen mixtures in an SI-engine: engine performance and analysis of a proposed fuel system. Fuel 2011;90(2):854–64. <https://doi.org/10.1016/j.fuel.2010.09.042>.
- [7] Westlye FR, Ivarsson A, Schramm J. Experimental investigation of nitrogen based emissions from an ammonia fueled SI-engine. Fuel 2013;111:239–47. <https://doi.org/10.1016/j.fuel.2013.03.055>.
- [8] Koike M, Miyagawa H, Suzuki T, Ogasawara K. Ammonia as a hydrogen energy carrier and its application to internal combustion engines. J Combust Soc Japan 2016;58(184):99–106. https://doi.org/10.20619/jcombsj.58.184_99.
- [9] Lhuillier C, BREQUIGNY P, Contino F, Rousselle C. Combustion Characteristics of Ammonia in a Modern Spark-Ignition Engine; 2019. SAE Technical Paper 2019-24-0237. <https://doi.org/10.4271/2019-24-0237>.
- [10] Mounaim-Rousselle C, Mercier A, Brequigny P, Dumand C, Bouriot J, Houillé S. Performance of ammonia fuel in a spark assisted compression Ignition engine. Int J Engine Res 2021;23(5):781–92. <https://doi.org/10.1177/14680874211038726>.
- [11] Niels Förby, Thomsen TT, Rasmus Faurskov Cordtz, Frantz Bræstrup and Schramm J. Ignition and combustion study of premixed ammonia using GDI pilot injection in CI engine 2023;331:1–9. <https://doi.org/10.1016/j.fuel.2022.125768>.
- [12] Reiter AJ, Kong S-C. Combustion and emissions characteristics of compression-ignition engine using dual ammonia-diesel fuel. Fuel 2011;90(1):87–97. <https://doi.org/10.1016/j.fuel.2010.07.055>.
- [13] Frost J, Tall A, Sheriff AM, Schönborn A, Hellier P. An experimental and modelling study of dual fuel aqueous ammonia and diesel combustion in a single cylinder compression ignition engine. Int J Hydrogen Energy 2021;46(71):35495–510. <https://doi.org/10.1016/j.ijhydene.2021.08.089>.
- [14] Liu Z, Wei H, Shu G, Zhou L. Ammonia-hydrogen engine with reactivity-controlled turbulent jet ignition (RCTJI). 348, pp.128580–128580. <https://doi.org/10.1016/j.fuel.2023.128580>.
- [15] Alkidas AC. Combustion-chamber crevices: the major source of engine-out hydrocarbon emissions under fully warmed conditions. Prog Energy Combust Sci 1999;25(3):253–73. [https://doi.org/10.1016/s0360-1285\(98\)00026-4](https://doi.org/10.1016/s0360-1285(98)00026-4).
- [16] Smith P, Cheng WK, Heywood JS. Crevise Volume Effect on Spark Ignition Engine Efficiency; 2014. SAE Technical Paper 2014-01-2602. <https://doi.org/10.4271/2014-01-2602>.
- [17] Wentworth JT. The piston crevice volume effect on exhaust hydrocarbon emission. Combus Sci Technol 1971;4(1):97–100. <https://doi.org/10.1080/00102207108952475>.
- [18] Glarborg P, Dam-Johansen K, Miller JA. The reaction of ammonia with nitrogen dioxide in a flow reactor: implications for the NH₂ + NO₂ reaction. Int J Chem Kinet 1995;27(12):1207–20. <https://doi.org/10.1002/kin.550271207>.
- [19] Glarborg P. The NH₃/NO₂/O₂ system: constraining key steps in ammonia ignition and NO_x formation. Combust Flame 2022;1–9. <https://doi.org/10.1016/j.combustflame.2022.112311>.
- [20] Jespersen MC, Rasmussen TØH, Ivarsson A. Widening the operation limits of a SI engine running on neat ammonia. CIMAC 2023 – paper 606, Busan, Korea; 2023.
- [21] Wei H, Kolodziej CP, Choi S, Som S, Broatch A, Gomez-Soriano J, et al. Development of a virtual CFR engine model for knocking combustion. Analysis 2018;11(6):1069–82. <https://doi.org/10.4271/2018-01-0187>.
- [22] Eberhard SE, Munck L. CFD modelling of crevice flow and flame propagation of premixed methane combustion in a CFR engine. Technical University of Denmark; 2023. MS Thesis.,
- [23] Eng JA, Leppard WR, Najt PM, Dryer FL. Experimental hydrocarbon consumption rate correlations from a spark ignition engine. SAE Technical Paper 1997;972888. <https://doi.org/10.4271/972888>.
- [24] Oliveira IS, Hochgreb S. Effect of Operating Conditions and Fuel Type on Crevice HC Emissions: Model Results and Comparison with Experiments. SAE Technical Paper 1999-01-3578; 1999. <https://doi.org/10.4271/1999-01-3578>.
- [25] Goodwin DA, Speth RL, Moffat HK, Weber BW. Cantera: an object-oriented software toolkit for chemical kinetics. Thermodyn Transp Process 2018. <https://doi.org/10.5281/zenodo.1174508>.
- [26] Cerbe G, Hoffmann HJ. Einführung in die Thermodynamik - Von den Grundlagen zur technischen Anwendung. 11th ed. München, Wien: Carl Hanser Verlag; 1996.
- [27] Namazian M, Heywood JS. Flow in the piston-cylinder-ring crevices of a spark-ignition engine: effect on hydrocarbon emissions. Eff Power SAE Technical Paper 1982;820088. <https://doi.org/10.4271/820088>.